A Search for Radio Emission from Supernovae With Ages from About One Week to More Than 80 Years

Christopher R. Eck, John J. Cowan, and David Branch

Department of Physics and Astronomy, University of Oklahoma, Norman, OK 73019

Christopher_R_Eck@raytheon.com, cowan@mail.nhn.ou.edu, branch@mail.nhn.ou.edu

Received ______________________; accepted ______________________

ABSTRACT

We report VLA radio observations of 29 SNe with ages ranging from 10 days to about 90 years past explosion. These observations significantly contribute to the existing data pool on such objects. Included are detections of known radio SNe 1950B, 1957D, 1970G, 1983N, the suspected radio SN 1923A, and the possible radio SN 1961V. None of the remaining 23 observations resulted in detections, providing further evidence to support the observed trend that most SNe are not detectable radio emitters. To investigate the apparent lack of radio emission from the SNe reported here, we have followed standard practice and used Chevalier's "standard model" to derive (upper limits to) the mass-loss rates for the supernova progenitors. These upper limits to the fluxes are consistent with a lack of circumstellar material needed to provide detectable radio emission for SNe at these ages and distances. Comparison of the radio luminosities of these supernovae as a function of age past explosion to other well-observed radio SNe indicates that the Type II SNe upper limits are more consistent with the extrapolated light curves of SN 1980K than of SN 1979C, suggesting that SN 1980K may be a more typical radio emitter than SN 1979C. For completeness, we have included an appendix where the results of analyses of the non-SN radio sources are presented. Where possible, we make (tentative) identifications of these sources using various methods.

Subject headings: circumstellar matter — supernovae: general

1. INTRODUCTION

Supernovae have been observed visually and recorded for at least the last 1000 years (Clark & Stephenson 1982) but only in this century have we been able to observe these bright, energetic events in a waveband other than the optical. The different supernovae (SNe) are classified into two main Supernova (SN) Types, I and II, distinguished by features in their optical spectra. The presence or absence of other optical features classify SNe into several sub-classifications, SNe Ia, Ib, Ic, and some other proposed sub-classes (e.g., the SNe IIn [Schlegel 1990]). To understand SNe explosions and the mechanisms for the emission of radiation, it is helpful to have knowledge of the pre-SN progenitor system. While a basic understanding of the pre-SN progenitor stars has been achieved (e.g., Branch, Nomoto, & Filippenko 1991, Branch et al. 1995), the specifics are still a matter of some debate (e.g., Nomoto et al. 1996). Radio observations of SNe have been shown (e.g., Weiler et al. 1989) to give insight into the pre-SN progenitor system.

The first discovery of radio emission, from SN 1970G in NGC 5457 (M101) (Gottesman et al. 1972, Allen et al. 1976), introduced this new regime in which to study SNe. Modern detections of well-observed radio SNe include the Type II SNe 1978K in NGC 1313 (Ryder et al. 1993, Schlegel et al. 1999), 1979C in NGC 4321 (Weiler et al. 1986, Weiler et al. 1991, Montes et al. 2000), 1980K in NGC 6946 (Weiler et al. 1986, Weiler et al. 1992a, Montes et al. 1998), 1981K in NGC 4258 (Weiler et al. 1986, Van Dyk et al. 1992, Lacey et al. 1999), 1986J in NGC 891 (Rupen et al. 1987, Weiler, Panagia, & Sramek 1990), 1988Z in MCG +03-28-022 (Van Dyk et al. 1993b, Lacey et al. 1999), and 1993J in NGC 3031 (M81) (Van Dyk et al. 1994); the Type Ib SNe 1983N in NGC 5457 (Sramek, Panagia, & Weiler 1984, Cowan & Branch 1985) and 1984L in NGC 991 (Panagia, Sramek, & Weiler 1986); and the Type Ic SNe 1990B in NGC 4568 (Van Dyk et al. 1993a). Most of these SNe can now be considered as "intermediate-age" supernovae, originally defined by Cowan &

Branch (1985) to have an age between 10 and 100 years old. These decades-old supernovae are observed in the radio much after a supernova fades in the optical, typically within two years, and before the earliest turn on of an SNR, predicted to take at least 100 years (see also Cowan, Roberts, & Branch 1994 and Stockdale et al. 2001a, b for further discussion). Many of the detected "intermediate-age" SNe whose ages are greater than 30 years include SNe 1970G (Cowan, Goss, & Sramek 1991; Stockdale et al. 2001a), 1968D in NGC 6946 (Hyman et al. 1995), 1961V in NGC 1058 (Branch & Cowan 1985, Cowan, Henry, & Branch 1988, Stockdale et al. 2001b) [but there is some discussion on whether this was a SN explosion or the pulse of an LBV (e.g., Filippenko et al. 1995)], 1957D & 1950B in NGC 5457 (M83) (Cowan et al. 1994, Cowan & Branch 1985, Cowan & Branch 1982) and the probable radio SN 1923A (Eck et al. 1998).

The investigation of radio emission from Supernova Remnants (SNRs) has been well studied due in part to the the strength, nature and longevity of the emission. (While a review of radio emission from SNRs is beyond the scope of this paper, a review of the emission from SNRs can be found in Weiler & Sramek (1988) and Matonick & Fesen (1997)). Some examples of well-known galactic SNRs include SNR 1006, Kepler's SNR, and Tycho's SNR as well as many extra-galactic SNRs (Green 1984). One particular radio SNR of interest is Cas A (Baars et al. 1977), the remnant from an SN that exploded in approximately 1670. At about 300 years old, Cas A is significant to our study because it is the youngest radio SNR with a known age. It is therefore useful for comparison with observations of many of our older SNe in probing the relationship between radio SNe and SNRs.

Despite attempts to look for radio emission from all SN types, no Type Ia SNe have been detected (e.g., Eck et al. 1995, Sramek et al. 1993, Weiler et al. 1989), and most Type II or Ib/c SNe (i.e., core-collapse SNe) have not been detected as radio emitters despite several searches (e.g., Eck et al. 1996, Sramek et al. 1993, Weiler et al. 1989). However, when radio emission has been detected the Chevalier model (Chevalier [1982a,b], 1984) describes the radio emission and fits the data very well and may offer an explanation for the lack of detectable radio emission from every SN. In this model the radio emission is related to circumstellar matter. For older SNe that may be entering the SNR phase, theoretical models (Gull 1973) and calculations (Cowsik & Sarkar 1984) describe the radio emission as related to the amount of interstellar matter (among other parameters such as energy released in the explosion) instead of circumstellar matter, but the emission mechanisms in each case are similar. While the Gull model predicts a minimum time of about 100 years for a SNR to brighten, it is noteworthy that SN 1885A has not been detected in the radio (Crane et al. 1992) at an age of about 107 years.

In this paper, we present results of a long term survey to detect radio emission from SNe at ages from 7 days to almost 90 years old. Our results confirm the observed trend that most SNe at these ages do not show radio emission. In §2 we present our observations, and in §3 discuss our results as applied to the Chevalier model to derive (upper limits to) mass-loss rates. We then discuss our results in relation to others' observations and work. In §4, we follow with conclusions. In Appendix A we present the results of our analysis of the non-SNe sources in our maps, and attempt to identify the sources when possible.

2. OBSERVATIONS

This series of observations began in an attempt to detect radio emission from intermediate-age SNe. If detected, a monitoring program could begin at the Very Large

Array (VLA)[1] to trace the evolution from a radio supernova (RSN) into an SNR. Since there is very little data on the transition of RSNe to SNRs, these observations would help in understanding this phase of SN evolution.

All observations were taken at the VLA over a time span ranging from 1981 to 1995, and the SNe observed vary in distance and in ages at the time of observation. Tables 1-3 summarize relevant observational data for the SNe reported here. Table 1 gives parameters for each observation, and Table 2 shows distances assumed for each SN, most based on Cepheid observations in the parent galaxy or in a galaxy in the same group. Table 3 summarizes data on each SN, its parent galaxy, the age at the time of observation and the flux densities for detections or 3σ upper limits to detection. Table 4 presents the results of our analysis of the observational data (see §3.1 for discussion).

In addition to analyzing the region near the SNe sites, for completeness we analyzed the non-SNe sources to determine a probable identity based on superpositions with maps made at optical (Hα) wavelengths or on spectral indices, for example. Descriptions of the analyses of each map were appended to the paper as Appendix A to preserve the main focus of the paper on radio SNe. Table 5 lists the positions and fluxes for these non-SNe sources and a possible identity for each.

[1]The VLA is a facility of the National Radio Astronomy Observatory, which is operated by Associated Universities, Inc., under contract to the National Science Foundation.

3. DISCUSSION

3.1. The Model

To gain insights into the pre-SN progenitor system via radio emission, we begin with the expression for the radio luminosity for Type II SNe based on the well-established Chevalier (1982a,b) mini-shell model. According to this model, the outward moving shock from the SN explosion encounters circumstellar material, compresses it and creates Rayleigh-Taylor instabilities. The magnetic fields locked in the material compress and amplify, accelerating free electrons. Synchrotron radiation results and is responsible for the luminosity we see. This luminosity has the form (following Chevalier [1982b])

$$L \propto \left(\frac{\dot{M}}{w}\right)^{(\gamma-7+12m)/4} t^{-(\gamma+5-6m)/2} m^{(5+\gamma)/2} U^{3(1-m)} \nu^{-(\gamma-1)/2} e^{-\tau_{\nu,ff}} \tag{1}$$

where

$$\tau_{\nu,ff} = C \left(\frac{\dot{M}}{w}\right)^{(5-3m)} t^{-3m} \nu^{-2.1}, \tag{2}$$

$\dot{\mathrm{M}}$ is the mass-loss rate of the pre-SN progenitor in $\mathrm{M}_{\odot}$ yr^{-1}, w is the wind speed in km s^{-1}, γ is the electron energy index, related to the radio spectral index, α, by $\gamma = 2\alpha + 1$, t is the time since explosion in days, m is defined by the ratio $(n-3)/(n-2)$, and n is the power law index for the ejecta density profile defined by $\rho \propto r^{-n}$. U is a parameter that depends on the density of the supernova ejecta at a given ejecta speed, $\tau_{\nu,ff}$ is the frequency dependent optical depth due to free-free absorption experienced by the radio emission as it escapes outward from the interaction region into the surrounding circumstellar material, and C is a constant. Initially, the optical depth is large, depressing the emission, but as the shock moves out, the optical depth falls with circumstellar density and the radio emission peaks. Note that due to the frequency dependence of the optical depth, shorter wavelengths peak first. According to the model, after peaking the radio emission falls monotonically to undetectability. The radio emission may eventually rise again either from another phase of interaction with a denser layer of circumstellar material (e.g., SNe 1979C, 1987A) or from the onset of the SNR phase.

How does the model apply to different SN types? For core-collapse SNe (Type II, Ib/c) the interaction occurs between the outgoing shock and the pre-SN progenitor wind. For Type Ia SNe the interaction can take place between the outgoing shock front of the white dwarf explosion and the wind of a companion red giant (Boffi & Branch 1995, Eck et al. 1995). For detectable radio emission, there must be enough circumstellar material (high enough $\dot{\rm M}$/w) to fuel the synchrotron emission, so for small $\dot{\rm M}$/w (of the progenitor or companion) no strong radio emission is expected.

For detected SNe, the data follow this "standard model" very well (e.g., Weiler et al. 1986, Weiler et al. 1990, Van Dyk et al. 1992) albeit with occasional minor modifications such as periodicities folded into the model and interpreted (Weiler et al. 1991) to better fit the data. Calculations by Chevalier (1998) indicate that synchrotron self-absorption may be important for SNe Ib/c and SN 1987A as well as for SN whose progenitors have low mass-loss rates. Ignoring this effect may cause an overestimate of mass-loss rates.

By knowing the luminosity, the frequency and the age of an observation we may predict the mass-loss rate of the pre-SN progenitor provided we can determine the other parameters. Since most of our observations are non-detections (i.e., upper limits to flux densities), we do not have the data to determine all the parameters with a fitting routine. However, we may salvage the data by scaling the Type II SNe data to the parameters of the well-known SN 1979C and scaling the Type I SNe data to SN 1983N, a Type Ib with similar (derived) properties to another Type Ib, SN 1984L (This procedure is similar to one used by Weiler et al. 1989 to estimate (upper limits to) mass-loss rates for many other radio SNe (see §3.2.1)). Of course calculations performed in this way must be taken only as rough estimates since every SN is not exactly like SNe 1979C or 1983N. We are effectively forcing every SN in our data set to look like either SN 1979C or SN 1983N, which has only limited validity, but the results can be useful where no data were previously available.

We determined the relevant parameters for the mass-loss rate calculations in the following manner. A reasonable parameter for Type II SNe is $n = 20$ ($m = 0.94$) (Eck et al. 1996), and the radio spectral index for SN 1979C is $\alpha = -0.72$ ($\gamma = 2.4$) from Weiler et al. (1986). We may incorporate the constants K, U, and $m^{(5+\gamma)/2}$ into one constant and determine its value by substituting all other known parameters and solving. The constant C can be determined by knowing the optical depth, age, frequency and mass-loss rate of an observation. Weiler et al. (1986) have fitted data for SN 1979C to determine their parameter K_2, representative of the optical depth at 5 GHz and $t = 1$ day. Additionally, we use the mass-loss rate calculated by Weiler et al. (1986) for SN 1979C to calculate C. The resulting luminosity equation is

$$L = 1.8 \times 10^{37} \left(\frac{\dot{M}}{w/10 \text{ km s}^{-1}}\right)^{1.7} \left(\frac{t}{1 \text{ day}}\right)^{-0.88} \left(\frac{\nu}{5 \text{ GHz}}\right)^{-0.7} e^{-\tau_{\nu,ff}} \text{ erg s}^{-1} \tag{3}$$

where

$$\tau_{\nu,ff} = 2.6 \times 10^{16} \left(\frac{\dot{M}}{w/10 \text{ km s}^{-1}}\right)^{2.18} \left(\frac{t}{1 \text{ day}}\right)^{-2.8} \left(\frac{\nu}{5 \text{ GHz}}\right)^{-2.1} . \tag{4}$$

For Type I SNe, the SN density power law index is typically $n = 7$ ($m = 0.8$), and for SN 1983N, Weiler et al. (1986) report $\alpha = -1.03$ ($\gamma = 3.1$). Determining the other constants in the same manner for Type II SNe results in a luminosity equation for SNe Type I

$$L = 9.1 \times 10^{36} \left(\frac{\dot{M}}{w/10 \text{ km s}^{-1}}\right)^{1.4} \left(\frac{t}{1 \text{ day}}\right)^{-1.6} \left(\frac{\nu}{5 \text{ GHz}}\right)^{-1.0} e^{-\tau_{\nu,ff}} \text{ erg s}^{-1} \tag{5}$$

where

$$\tau_{\nu,ff} = 3.5 \times 10^{17} \left(\frac{\dot{M}}{w/10 \text{ km s}^{-1}}\right)^{2.6} \left(\frac{t}{1 \text{ day}}\right)^{-2.4} \left(\frac{\nu}{5 \text{ GHz}}\right)^{-2.1} \tag{6}$$

We take the commonly assumed value for the wind speed, 10 km s^{-1}. For simplicity we use this wind speed for all SN Types although we note that for Types Ib/c, the wind speed may be higher. Calculated values for $\dot{\rm M}$ are shown in Table 4. In many cases the observation age has been calculated from the time of maximum brightness or from the time of discovery since data on the explosion date was not available, especially for the older SNe. Thus, the ages may be in error by about 30 days. For any SNe (in our survey) with observation ages older than that of SN 1983K ($\sim$ 1500 days) this amounts to an error in the ages of less than 2%. For the SNe with observation ages less than 1500 days, we were able to obtain data on the explosion date for a better calculation of the (upper limit to the) mass-loss rate.

For all but two of the upper limits, the observation age is large enough that the radio emission can be assumed to be fading (for the purposes of deriving a mass-loss rate.) However, observations for the Type Ia SNe 1986G and 1989B are at 10 and 14 days past explosion, respectively. It is possible that the radio emission at these ages could be rising (pre-peak) or falling (post-peak). This would result in two different derived mass-loss rates—a larger mass-loss rate corresponding to the optically thick case when the emission has not peaked yet and a smaller mass-loss rate corresponding to the optically thin case when the emission has already peaked (see Eck et al. 1995 for details and previously published results for a similar case of early observations of SN 1986G). For SNe Ia we may be able to test whether the progenitor system is a symbiotic (white dwarf accreting matter from the wind of a red giant companion) using early radio observations such as these. By comparing the range of derived mass-loss rates to the mass-loss rate expected from red giants in symbiotic systems (10^{-7} to 10^{-5} $M_\odot$ yr^{-1} [Seaquist & Taylor 1990, Mürset et al.

1991]) we may test the symbiotic scenario. Inspection of Table 4 reveals that the derived range of mass-loss rates for SNe 1986G and 1989B are in mild conflict with that expected for the symbiotic red giant companion (in agreement with original calculations by Eck et al. [1995] for SN 1986G). These were probably not symbiotic systems.

3.1.1. Model Assumptions

We now examine some of the assumptions in the Chevalier model and their possible effects on the derived luminosities and mass-loss rates. One of the key assumptions in the theory of the origin of the synchrotron radio luminosity concerns the efficiency of conversion of the thermal energy density of electrons into the magnetic energy density and relativistic electron energy density. It has been assumed that this value is constant at about 1% (Chevalier 1982b), but this assumption is being questioned based on observations of SN 1987A. Also inherent is the assumption that the density of the circumstellar wind material and the outer layers of the SN ejecta are described by time-independent power laws, $\rho_{csm} \propto r^{-2}$ and $\rho_{SN} \propto r^{-n}$. While the assumptions on the density profile of the SN ejecta have been shown to be good assumptions, some cases have shown evidence for a circumstellar power law density that looks different from the assumed form, i.e. $\rho_{csm} \propto r^{-3/2}$ (SN 1993J: Van Dyk et al. 1994). This has been interpreted as a changing presupernova mass-loss rate. Other radio SNe have shown evidence for clumpiness in the pre-SN wind or non-spherical symmetry of the shock and a mix of internal absorbers and emitters along the line of sight (SNe 1986J: Weiler et al. 1990, SN 1988Z: Van Dyk et al. 1993b). In these particular cases, the model was modified to better fit the data. Finally, if synchrotron self-absorption is important, the derived upper limits to mass-loss rates may be overestimated (Chevalier 1998). Since these are only upper limits, we do not include these effects.

For detected SNe with enough data to form a light curve, mass-loss rates can be derived directly. Equation (16) from Weiler et al. (1986) gives an expression for the mass-loss rate as a function of several parameters, one of which, τ_{ff}, the free-free optical depth, can be derived by fitting the data. Some common assumptions on the other parameters are $v_{shock} = 10^4$ km s^{-1}, $v_{wind} = 10$ km s^{-1}, and $T_e = 10^4$ K in the wind. How sensitive are the mass-loss rates to these values? While the functional form for the dependence of these parameters on the mass-loss rate is obvious from the expression from Weiler et al. (1986), there are other considerations. For example, Lundqvist & Fransson (1988) report that the assumption of a fully ionized wind may underestimate the mass-loss rate by a factor of 2 or more. To review this and some other considerations affecting the radio emission, we refer the reader to Lundqvist & Fransson (1988).

In the calculation of the (upper limits to) mass-loss rates for Type I SNe, we have assumed that the Type Ib/c and Type Ia SNe share model parameters. Despite the lack of detections of Type Ia SNe, we have followed Weiler et al. (1989) and performed calculations using this assumption in an effort to salvage our data on Type Ia SNe.

3.2. Comparisons

3.2.1. Other Radio SN Searches

Montes et al. (1997) reported a detection of SN 1986E at an age of about 8 months. By scaling some of the parameters to those of SNe 1979C & 1980K and using the detection of SN 1986E as well as some tight upper limits, they derive a light curve and a subsequent mass-loss rate of $> 4.7 \times 10^{-5}$ M$_\odot$ yr^{-1}. While our upper limits are consistent with their radio light curve (i.e., their derived radio light curve predicts the radio emission to be less than our upper limits at the epochs of our observation), our derived mass-loss rate appears to be in conflict, at $< 4.9 \times 10^{-6}$ M$_\odot$ yr^{-1}, by an order of magnitude. However, there are several items to be noted in comparing the results of Montes et al. and the results found here. First, Montes et al. apparently derive the mass-loss rate using only the free-free absorption term (equation 2, here) while a somewhat different form has been used in our calculation, i.e., both equations 1 and 2. It is also noted that for most of the epochs of our observations, the mass-loss rate derives mainly from equation 1 since it is probable that optical depth is very small. Second, by using the Montes et al. detection and our parameters for Type II SNe, we find two mass-loss rates: one corresponding to the optically thick case (6.5×10^{-5} M$_\odot$ yr^{-1}) and one corresponding to the optically thin case (4.1×10^{-6} M$_\odot$ yr^{-1}). It is unclear whether SN 1986E is pre-peak (optically thick) or post-peak (optically thin) at the epoch of the Montes et al. observation and therefore unclear whether there is a conflict between our results and Montes et al. A calculation using the Montes et al. upper limits in the same manner restricts the mass-loss rates to be 2.1×10^{-6} M$_\odot$ yr^{-1} $< \dot{\mathrm{M}} <$ 1.2×10^{-5} M$_\odot$ yr^{-1} at the earliest epochs ($<$ 200 days) and $\dot{\mathrm{M}} <$ 4.4×10^{-6} M$_\odot$ yr^{-1} at the later epochs ($>\sim$ 200 days). Third, the epochs of Montes et al. observations and ours are separated by $\sim 6 - 8$ years. (It is unlikely that SN 1986E is still in an optically thick phase at the epochs of our observation since unreasonably high mass loss rates ($> 10^{-3}$ M$_\odot$ yr^{-1}) are required using our model parameters. Only the optically thin result has been quoted here).

Our upper limit to the pre-SN mass-loss rate for SN 1986E is consistent with the Montes et al. observation if the SN was in an optically thin phase at both epochs. If the SN was in an optically thick phase at the Montes et al. epoch, there appears to be a conflict between our model results and theirs, however there is some evidence for a changing pre-SN mass-loss rate in other SNe (e.g., SN 1993J Van Dyk et al. 1994).

To analyze the sensitivity of the calculation to the model parameters, we calculate the mass-loss rate for all of the upper limits and observations of SN 1986E by scaling to the Montes parameters and by scaling to SN 1979C. For the same observation, the (upper limits to) mass-loss rates are lower by a factor of $5 - 10$ by scaling to SN 1979C versus scaling to SN 1986E. This indicates that the assumptions on parameters are important and that our results may only be accurate to within an order of magnitude, but again our results can be useful where no other data is available.

Brown & Marscher (1978) report radio upper limits to 46 SNe at two wavelengths and at ages varying from a few months to more than 70 years. Their sample contains many of the SNe in the present sample (SNe 1895B, 1909A, 1921B, 1921C, 1937F, 1951H, 1954J, 1959D, 1961V, 1969L, 1970G, 1972E and 1973R), but with relatively high upper limits (by today's standards) in the range $3 - 30$ mJy; they reported no detections. By applying our models to their data on upper limits, we may derive upper limits to mass-loss rates similarly to what we have done with our own data. Despite some early observations from Brown & Marscher at less than a year after explosion, no upper limits to mass-loss rates were obtained that are lower than ours.

Weiler et al. (1989) first performed a procedure very similar to what we have done in calculating upper limits to mass-loss rates for 24 SNe observed by them at 6 cm, including SNe I and II. They calculate mass-loss rates by scaling all Type II to SNe 1979C & 1980K and all Type I to SN 1983N, but they do not include absorption effects (except for the fluxes from SNe 1979C & 1980K). At late times absorption is negligible, but it can be important at earlier epochs. By not including an absorption term, this could cause an underestimate in mass-loss rates. We calculate mass-loss rates for the 24 SNe in Weiler et al. (1989) and derive upper limits that are $10\% - 60\%$ greater than theirs for their Type II SNe. For the Type I SNe in Weiler et al. (1989), including absorption effects depresses the emission enough that any physically reasonable mass-loss rate would have produced emission below the flux density upper limits for many of their older, more distant SNe. For the closer Type I SNe observed early enough to restrict mass-loss rates, our upper limits to the mass-loss rates are greater than theirs. The $10\% - 60\%$ differences in the results from applying our model to Weiler et al. upper limits are likely mainly due to free-free absorption effects, but could also be due to parameter differences.

3.2.2. Radio and optical emission

Can radio emission be predicted? Since radio emission is the result of shock-circumstellar matter interaction (radio SNe) or shock-interstellar matter (radio SNR) interaction, any evidence for circumstellar/interstellar interaction (in other wavebands) at SNe sites might be used as a predictor for radio emission.

Since most SNe have faded in the optical by an age of about 2 years, indications of optical emission beyond 2 years may be the result of some type of enhanced circumstellar interaction. There are 12 SNe that have been detected in the optical at an age of greater than 2 years. Of these, SN 1885A is the only Type Ia, with optical detection at 103 yrs (Fesen, Hamilton, & Saken 1989, Fesen 1997). However, since SN 1885A has been detected in the optical via absorption, there is no evidence for circumstellar interaction, so we remove it from our group of 12. All other SNe with evidence for optical emission at ages greater than 2 years are core-collapse SNe: SN 1957D at 30-32 yrs (Long, Blair, & Krzeminski 1989), SN 1961V at 22-24 yrs (Goodrich et al. 1989), SN 1970G at about 22 yrs (Fesen 1993), SN 1978K at 12-20 years (Ryder et al. 1993, Chugai, Danziger & Della Valle 1995; Chu et al. 1999, Schlegel et al. 1999), SN 1979C at 10 yrs (Fesen & Matonick 1993), SN 1980K at 7-9 yrs (Fesen & Becker 1990), SN 1985L at 12 yrs (Fesen 1998), SN 1986E at 7-8 yrs (Cappellaro, Danziger, & Turatto 1995), SN 1986J at 4-7 yrs (Leibundgut et al. 1991), SN 1987A at about 10 years (Sonneborn et al. 1998), and SN 1988Z up to 8.5

years (Aretxaga et al. 1999). Some of these SNe with optical recoveries have been observed to be radio emitters. SN 1987A has been detected in the radio at an age of about 10 yrs but at a flux level that would be undetectable at much greater distances. SNe 1957D and 1961V were recovered in the optical only after detection in the radio. (It is not clear whether SN 1961V was an SN or an LBV outburst [Goodrich et al. 1989, Filippenko et al. 1995], although recent radio observations support a supernova interpretation Stockdale et al. 2001b). SN 1970G was optically recovered shortly after the last radio detection (Cowan et al. 1991) which indicated a steep decline rate in the radio when combined with initial radio observations (Gottesman et al. 1972, Allen et al. 1976). Schlegel et al. (1999) report fading radio emission from SN 1978K since 1992 and report observations that indicate the optical light curve approaching a constant apparent magnitude starting at about 10 years past explosion. Observations of SN 1979C indicated fading radio emission (albeit with approximate sinusoidal variations [Weiler et al. 1992b]) at the time of optical recovery, but more recent observations indicate that it is now brightening in the radio (Montes et al. 2000). SN 1980K was optically recovered when the radio emission was fading, and recent radio results now indicate a sharper drop than previously reported (Montes et al. 1998) despite continued optical detections (Fesen, Hurford, & Matonick 1995). There is no available radio data SN 1985L at an age of greater than 3 yrs, but 6 cm data indicated fading emission near that time (Van Dyk et al. 1998). Although still fading from its initial rise, SN 1986J was emitting strongly in the radio at an age of 6 yrs. SNe 1885A (Crane, Dickel, & Cowan 1992) and 1986E (Eck et al. 1996) do not show detectable radio emission near the time of optical recovery although SN 1986E did show one radio detection at an age of 8 months (Montes et al. 1997). Observations of SN 1988Z show strong radio emission at an age of about 5 years (Van Dyk et al. 1993b). Model fits to the data at 5 years imply post-peak radio emission at 2, 3.6, and 6 cm but not at 20 cm (Van Dyk et al. 1993b). The optical light curve for SN 1988Z shows strong but generally fading optical emission

(Aretxaga et al. 1999) in this same epoch.

To summarize: of all 11 SNe (without SN 1885A) with optical recoveries, 9 show radio emission. Of these 9, only two (SNe 1979C and 1987A) show a rise in radio emission within a few years after optical recovery. It is unlikely that SNe 1979C and 1987A are entering a radio SNR phase at an age of only 10-20 yrs. Thus, optical recovery precedes an increase in radio emission while still in a RSN phase only for SNe 1979C and 1987A. Is optical recovery a good indicator (in general) of radio emission as the SN shock encounters circumstellar material? For a majority of the cases (9 out of 11), it would seem to be true. Support for a general correlation between late-time optical and radio emission is found in the behavior of SN 1957D, which showed a dramatic drop in the optical (Long, Winkler & Blair 1992) and contemporaneously in the radio (Cowan et al. 1994). A similar correlation was seen for SNe 1979C and 1980K between a leveling (SN 1979C) or drop (SN 1980K) in radio (Montes et al. 2000, 1998) and the behavior of the optical emission (Fesen et al. 1999). Although both radio and late-time optical emission (e.g., see Fesen et al. 1999 for discussion) may be indicative of enhanced circumstellar interaction, we caution that the emission mechanisms are different, as may be the regions where the emission originates. Clearly, further combined radio and optical studies will be required to understand better the long-term radio and optical correlations.

3.3. Luminosity-Age Plots

Figures 1 – 5 are plots of the radio luminosities for (3σ) upper limits versus age of observation for all of the SNe in our sample. The plots are separated by SN Type and wavelength. Each plot shows upper limits (as upside-down triangles), detections (larger unfilled polygons), and at least one SN of the same type with its model light curve (solid and dashed curves) and observational data (smaller unfilled circles). Because of its unknown

SN type, SN 1945B (Liller 1990) was included on both Type I and II SN plots. Although SNe 1950B and 1957D are both of unknown type, they are likely to be Type II SNe (Cowan et al. 1994, Eck et al. 1998) and were included only in the Type II plots.

3.3.1. Type II SNe

Inspection of the Type II plots at both 20 and 6 cm reveal that upper limits for SNe 1980D, 1984E & 1986E are below the data for SN 1979C but above the data for SN 1980K. Given that the radio emission from SN 1980K has fallen sharply, it is possible that most of the other upper limits (for the older SNe) have fluxes above that of SN 1980K. Recent data from Montes et al. (1998) indicate that radio emission from SN 1979C is now rising again instead of continuing to fade. The inconsistency of our upper limits and detections with the SN 1979C data and possible similarities with the SN 1980K data indicate that the Type II SNe in our survey have properties more like SN 1980K than SN 1979C. It also suggests that SN 1980K may be a more typical Type II radio emitter than SN 1979C.

3.3.2. Type I SNe

The observation age of SN 1895B makes it interesting to consider. We may compare it with model curves (dashed curves) for the radio turn-on of a SNR as calculated by Cowsik & Sarkar (1984). The dashed curves correspond to their models c) (constant density piston) and d) (isothermal piston) and assume an explosion energy of 10^{51} ergs, 0.5 solar masses of ejected material, an interstellar density of 1 baryon cm^{-1} and a spectral index, $\alpha \simeq -1$. It is clear that SN 1895B *could* be in the SNR phase, but the high upper limit does not exclude the possibility that it may still be fading as an RSN. At 6 cm, our data is very limited for Type I SNe. Since no Type Ia SNe have been detected in the radio, we cannot conclude much about the comparison of the upper limits and the SN 1983N light curve, except that our upper limits are below the light curve. For the 3.6 cm plot, no data was available for SN 1983N so we plot data and curves from the only other Type I SN with 3.6 cm data, the Type Ic SN 1990B. Without other radio light curves to compare our upper limits to, it is difficult to say anything with confidence about the upper limits (for the Type Ia SNe 1885A and 1989B) except that they are in mild conflict with the SN 1990B data.

4. CONCLUSIONS

We summarize the results of the analysis of the radio observations in our survey. Many of the conclusions found from analysis of our observations agree with and confirm conclusions found in other radio SNe papers (e. g. , Weiler et al. 1989). These observations increase the size of the data pool on radio observations of SNe and provide more data with which to test theories of radio emission from SNe.

1. Most SNe are not detectable radio emitters with current radio telescopes due to either large distances or intrinsically faint radio supernovae (or early enough observations).

2. No Type Ia SNe have been detected despite some early and/or deep observations (SNe 1885A [Crane et al. 1992], 1895B, 1937C, 1986G, 1989B).

3. While most of the Type II SNe observed in our survey were *not detected* in the radio, we find that most of the *detected* ones (of all the SN types) are Type II SNe.

4. Assuming the Chevalier model, our flux upper limits imply a lack of circumstellar material (or fuel) for detectable radio emission. Radio emission is thus dependent on pre-SN mass-loss and on mass-loss history.

5. Using the Chevalier model for Type Ia SNe, one scenario for which we could get radio emission is the symbiotic-star progenitor scenario (Boffi & Branch 1995). Our non-detections of SNe 1986G and 1989B indicate that the derived upper limits to mass-loss rates are in mild conflict with the mass-loss rates inferred from red giants in symbiotic systems. These SNe are probably not symbiotics. The other Type Ia SNe (SNe 1885A [Crane et al. 1992], 1895B, 1937C) have higher upper limits to the mass-loss rates so that we cannot discount the symbiotic-star scenario as a progenitor scenario.

6. By applying the Chevalier model to our Type II SNe observations, we see that no Type II SNe have been detected with a derived value for the mass-loss rate of $\dot{\mathrm{M}} \lesssim 10^{-6}\ \mathrm{M}_\odot\ \mathrm{yr}^{-1}$, implying a lack of circumstellar material. This value is very dependent on the scaling of the parameters of our SNe to those of the well-observed SN 1979C, and the uncertainty in our derived mass-loss rates may be as high as a factor of 10 due to dependencies on parameters (see SN 1986E).

7. The derived mass-loss rates can also have a dependence on the assumptions inherent in the Chevalier model. The effects of these assumptions on the radio luminosity are not trivial to calculate and warrant further study (e.g., see Lundqvist & Fransson [1988] for an investigation of some of these effects).

8. There are 11 SNe with optical recoveries (indicating circumstellar interaction) at an age of greater than 4 years. Of the SNe with optical recoveries, 9 have been detected as radio emitters (and for 2 cases of these 9, the optical emission preceded a second rise of radio emission). This implies that radio emission may be associated with optical recovery.

9. Since the upper limits for Type II SNe in our survey are more consistent with SN 1980K than with SN 1979C, these Type II SNe in our survey may have radio

properties more similar to SN 1980K than SN 1979C.

Finally, we note that despite more than two decades of theoretical and observational work in radio supernovae, radio emission from supernovae is not completely understood. As the intermediate-age radio supernovae are followed, we hope to explore further the transition of radio supernovae into supernova remnants. More sensitive observations of young and intermediate-age SNe, as well as more theoretical work, are needed to help us fully understand the origin and evolution of RSNe.

We would like to thank the anonymous referees for helpful comments and suggestions, Schuyler Van Dyk for sharing his optical Hα maps with us, Paul Hodge for providing positions of H II regions, Bill Romanishin for observing and reducing optical data on NGC 3627 for us, Kurt Weiler for helpful discussions, W. Miller Goss for providing the raw data on SN 1951H, Pat Crane for the upper limit on SN 1885A and Doug Roberts for help on the data analysis using AIPS. This work has been supported in part by NSF grants AST-9986974 and AST-9618332 at the University of Oklahoma.

This research has made use of the NASA/IPAC Extragalactic Database (NED) which is operated by the Jet Propulsion Laboratory, California Institute of Technology, under contract with the National Aeronautics and Space Administration.

Appendix A. Non-Supernova Radio Sources

To ensure completeness, but not take away from the focus of the paper, we have included this appendix as a description of the analysis of the non-SN radio sources in our maps. The non-supernova radio sources detected in our observations are listed in Table 5. Selected maps with more than 3 sources can be found in Figures 6 to 9. All peak fluxes and positions were determined by using AIPS (Astronomical Image Processing System provided by the NRAO) to fit the source to a two-dimensional Gaussian on top of a linearly sloping background. The fit to sources ϵ and π in NGC 3627 failed to report an uncertainty in flux, so we report the rms noise as representative of the flux uncertainty.

Many sources have been identified as H II regions via superposition onto Hα maps or via comparison with published positions of H II regions, but some caution must be exercised. Without a spectral index to verify the thermal nature of the radiation from these sources, we can only tentatively identify the radio emission as originating in the H II regions. (Consider the case of SN 1957D whose emission was initially non-thermal. Later measurements indicated that the emission is thermal and is believed to have faded below that of an associated H II region [Cowan et al. 1994].)

NGC 1058 Radio detection of SN 1961V has been reported by Cowan et al. (1988), Cowan & Branch (1985), and Cowan et al. (1991). An Hα map from Cowan et al. (1988) was available for comparison with our sources, but α had a position outside ($> 4'$ from galaxy center) the Hα field of view. On the other hand, β was within the field of view for the Hα map but did not correspond to any Hα emission region.

NGC 2403 A contour map of the radio sources in NGC 2403 can be seen in Figure 6. We detected 15 sources with a signal-to-noise of 5σ or greater. Turner & Ho (1994) report 6 cm radio observations of NGC 2403, including 7 sources whose positions lie within $1''$ to $5''$ of a corresponding source found in our 20 cm map. However, spectral index calculations were not possible since none of the mutually observed sources had the same beamsize and none were unresolved. Examination of integrated fluxes reveals that source β is consistent with thermal emission.

A map of H II regions from Sivan et al. (1990) superimposed onto our radio map reveals that β lies directly over a group of H II regions (including No. 293 in Sivan et al. 1990). Source β is likely a group of H II regions. The same positional coincidence with a radio source and an H II region(s) is found for sources γ, δ, ϵ, ρ, θ, ω, η, χ and ξ. They are likely H II regions as well. We find that the luminosities of these sources is comparable to H II regions identified in Cowan et al. (1994).

Comparison with reported SNRs in NGC 2403 by Matonick & Fesen (1997) reveals that source μ has a peak position very close to that of SNRs No. 6 & 7. At a distance of 3.2 Mpc to NGC 2403 (see Table 2), μ is about 50 pc from both SNRs No. 6 & 7. Since SNR No. 7 has a reported diameter of 60 pc, it is very possible that μ is identified with this SNR. More radio observations are recommended to confirm this identification.

NGC 3169 The first source in the list has a position that is coincident with the central regions of NGC 3169. The emission is probably associated with the center of the galaxy.

NGC 3627 Prior observations of NGC 3627 were found in Hummel et al. (1987) (1.49 GHz), Crane (1977) (2.7 & 8.1 GHz), Zhang, Wright, & Alexander (1993) (CO and H I) and Hodge (1974) (optical H II). Source α has a non-thermal spectral index and a position within the uncertainty ($10''$) for the galactic center. It lies directly over the CO peak in the center of the galaxy from Zhang et al. (1993) and is probably associated with the galactic center. Hummel et al. observe a source $< 0\farcs5$ from α with an integrated flux over the inner $2''$ of 15 ± 2 mJy. We measure the integrated flux over approximately the same region to be 12.5 ± 0.1 mJy.

Hα observations taken on the 18-inch telescope at University of Oklahoma by W. Romanishin (1997) reveal an emission region lying over β.

Hodge (1974) reports observations of H II regions expressed as offsets and plots them relative to the galactic center. If we superpose α with the position for the galactic center on the plot, we find that β lies directly over two H II regions (No. 12 & 13 in Hodge) indicating that β may be an H II region. Source γ has no counterpart in Hodge (1974).

Source ϵ has a position that is coincident with the position of an H II region (No. 47) reported by Hodge (1974). This coincidence assumes that the center of the galaxy is at α. Examination of the fluxes at two wavelengths indicates that the emission from ϵ is non-thermal. This probably indicates that there is an SNR nearby or possibly associated with the H II region. If we again assume that α is the center of the galaxy, we find that π lies $4''$ from the position of an H II region (No. 50), so it is not clear whether π is associated with an H II region or not.

NGC 4214 A contour map of most of the sources in this galaxy can be seen in Figure 7. There were at least 8 radio sources in this irregular galaxy with one (η) apparently composed of a number of smaller sources. Using an Hα map of the galaxy provided by Van Dyk (1997) and superposing our radio map with it, we can attempt to identify probable H II regions. Sources α, β, γ, ϵ and η have excellent positional coincidences with Hα emitting regions and are all probably H II regions. Hartmann, Geller, & Huchra (1986) list positions of H II regions, and their source H59 lies $3''$ from the peak position of source ρ. This source is likely to be an H II region. In addition, the Hartmann et al. (1986) source H48 lies $3''$ from the strongest source in the η complex. H54 & H55 lie close ($5\farcs5$ and $2''$, respectively) to the peak positions of β and α to make their identification probable.

NGC 4302 Analysis of the sources in this galaxy were originally reported in Eck et al. (1996).

NGC 4688 Superposition of the Digital Sky Survey (DSS) R-band image onto our radio map reveals no source coincident with the only prominent radio feature in our map.

NGC 5128 We report measurements of the radio bright center of NGC 5128 (Cen A) at 6 and 2 cm. The integrated fluxes are 6.1 Jy and 0.38 Jy at 6 and 2 cm, respectively and the resulting spectral index is $\alpha_2^6 = -2.5$.

NGC 5457 (M 101), S A map of the (southern) region surrounding NGC 5455 and containing many of the sources can be seen in Figure 8. SN 1970G is visible as a prominence pointing to the northwest from α. Source α has a flat spectral index and an excellent positional coincidence with NGC 5455, a known H II region. Sources δ and ω have spectral indices between 0.0 and 0.1 indicating they are likely H II regions as well. If we compare the positions of our sources with those of H II regions found by Hodge et al. (1990), we find positional coincidences (within the uncertainties) for ψ, ρ, θ, ϵ and δ. These are also probable H II regions. Comparison of the positions of SNRs in M 101 reported by Matonick & Fesen (1997) with our sources reveals no positional coincidences.

NGC 5457 (M 101), E A map of the eastern region of M 101 (containing the site of SN 1951H) can be seen in Figure 9. Prominent features include emission regions from the H II regions NGC 5461 & 5462. Superposition of the radio map with Hα maps found in Israel, Goss, & Allen (1975) reveals that sources κ, η, ϕ, and χ in NGC 5461 lie over Hα emission regions. The same positional coincidence is found for γ, ϵ, δ, β and α in NGC 5462. All of these are probable H II regions. The positions of our sources can be compared to H II regions observed by Hodge et al. (1990). We find that π, η, ϕ, γ, ϵ and α have peak positions that are within the uncertainties for the H II regions. In addition, λ, κ, χ, δ, β and θ have peak positions within twice the uncertainties of a particular H II region. The

Hodge et al. (1990) data indicate that these sources *may* be H II regions.

Both comparisons indicate that κ, η, ϕ, χ, π, γ, ϵ, δ, β and α are all probable H II regions.

Comparison with SNRs in M 101 from Matonick & Fesen (1997) shows no SNRs coincident with positions of any of our sources in the eastern region of M 101.

IC 4182 There are two prominent sources (α and β) in the west side of the radio map. Comparison with the VLA survey Faint Images of the Radio Sky and Twenty-centimeters (FIRST) [Becker, White, & Helfand 1995] reveals two sources in that survey with peak positions within $2\farcs5$ and $1\farcs0$ of α and β, respectively. These are very likely to be the same sources. Willis, Oosterbaan, & de Ruiter (1976) conducted a Westerbork Synthesis Radio Telescope (WSRT) survey including IC 4182 and observe two sources whose positions are within $3''$ and $11''$ of α and β, respectively, although the peak fluxes are somewhat larger.

REFERENCES

Allen, R. J., Goss, W. M., Ekers, R. D., & de Bruyn, A. G. 1976, A&A, 48, 253

Aretxaga, I., Benetti, S., Terlevich, R. J., Fabian, A. C., Cappellaro, E., Turatto, M., & Della Valle, M. 1999, MNRAS, 309, 343

Baars, J. W. M., Genzel, R., Pauliny-Toth, I. I. K., & Witzel, A. 1977, A&A, 61, 99

Becker, R. H., White, R. L., & Helfand, D. J. 1995, ApJ, 450, 559

Boffi, F. R. & Branch, D. 1995, PASP, 107, 347

Branch, D., & Cowan, J. J. 1985, ApJ, 297, L33

Branch, D., Nomoto, K., & Filippenko, A. V. 1991, Comments Astrophys., 15, 221

Branch, D., Livio, M., Yungelson, L. R., Boffi, F. R., & Baron, E. 1995, PASP, 107, 1019

Brown, R. L., & Marscher, A. P. 1978, ApJ, 220, 467

Cappellaro, E., Danziger, I. J. & Turatto, M. 1995, MNRAS, 277, 106

Chevalier, R. A. 1982a, ApJ, 258, 790

Chevalier, R. A. 1982b, ApJ, 259, 302

Chevalier, R. A. 1984, ApJ, 285, L63

Chevalier, R. A. 1998, AJ, 499, 810

Chu, Y-H., Caulet, A., Montes, M. J., Panagia, N., Van Dky, S. D., Weiler, K. W., 1999, ApJ, 512, L51

Clark, D. H., & Stephenson, F., R. 1982, in Supernovae: A Survey of Current Research, eds. M. J. Rees & R. J. Stoneham (D. Reidel Publishing Company), p. 355

Cowan, J. J., & Branch, D. 1982, ApJ, 258, 31

Cowan, J. J., & Branch, D. 1985, ApJ, 293, 400

Cowan, J. J., Henry, R. B. C., & Branch. D. 1988, ApJ, 329, 116

Cowan, J. J., Goss, W. M., & Sramek, R. A. 1991, ApJ, 379, L49

Cowan, J. J., Roberts, D. A., & Branch, D. 1994, ApJ, 434, 128

Cowsik, R., & Sarkar, S. 1984, MNRAS, 207, 745

Crane, P. C. 1977, Thesis, Massachusetts Institute of Technology

Crane, P. C., Dickel, J. R. & Cowan, J. J. 1992, ApJ, 390, L9

Donnelly, R. H., Partridge, R. B. & Windhorst, R. A. 1987, ApJ, 321, 94

Eck, C. R., Cowan, J. J., Roberts, D., Boffi, F. R., & Branch, D. 1995, ApJ, 451, L53

Eck, C. R., Cowan, J. J., Boffi, F. R., & Branch, D. 1996, ApJ, 472, L25

Eck, C. R., Roberts, D. , Cowan, J. J., & Branch, D. 1998, ApJ, in press

Fesen, R. A., Hamilton, A. J. S. & Saken, J. M. 1989, ApJ, 341, L55

Fesen, R. A. & Becker, R. H. 1990, ApJ, 351, 437

Fesen, R. A. 1993, ApJ, 413, L109

Fesen, R. A. & Matonick, D. M. 1993, ApJ, 407, 110

Fesen, R. A., Hurford, A. P. & Matonick, D. M. 1995, AJ, 109, 2608

Fesen, R. A. 1997, BAAS, 29, 1268

Fesen, R. A. 1998, AJ, 115, 1107

Fesen, R. A., Gerardy, G. L., Filippenko, A. V., Matheson, T., Chevalier, R. A., Kirshner, R. P., Schmidt, B. P., Challis, P., Fransson, C., Leibundgut, B., & Van Dyk, S. D., 1999, AJ, 117, 725

Filippenko, A. V., Barth, A. J., Bower, G. C., Ho, L. C., Stringfellow, G. S., Goodrich, R. W., & Porter, A. C. 1995, AJ, 110, 2261

Goodrich, R. W., Stringfellow, G. S., Penrod, G. D., & Filippenko, A. V. 1989, ApJ, 342, 908

Gottesman, S. T., Broderick, J. J., Brown, R. L., Balick, B., & Palmer, P. 1972, ApJ, 174, 383

Green, D. A. 1984, MNRAS, 209, 449

Gull, S. F. 1973, MNRAS, 161, 47

Hartmann, L. W., Geller, M. J., & Huchra, J. P. 1986, AJ, 92(6), 1278

Hodge, P. W. 1974, ApJS, 27, 114

Hodge, P. W., Gurwell, M., Goldader, J. D., & Kennicutt, R. C., Jr. 1990, ApJS, 73, 661

Hughes, S. M. G., Mingsheng, H., Hoessel, J., Freedman, W. L., Kennicutt, Jr., R. C., Mould, J. R., Saha, A., Stetson, P. B., Madore, B. F., Silbermann, N. A., Harding, P., Ferrarese, L., Ford, H., Gibson, B. K., Graham, J. A., Hill, R., Huchra, J., Illingworth, G. D., Phelps, R. & Sakai, S. 1998, in press

Hummell, E., van der Hulst, J. M., Keel, W. C., & Kennicutt, R. C., Jr. 1987, A&AS, 70, 517

Hyman, S. D., Van Dyk, S. D., Weiler, K. W., & Sramek, R. A. 1995, ApJ, 443, L77

Israel, F. P., Goss, W. M., & Allen, R. J. 1975, A&A, 40, 421

Kelson, D. D., Illingworth G. D., Freedman, W. F., Graham, J. A., Hill, R., Madore, B. F., Saha, A., Stetson, P. B., Kennicutt, Jr., R. C., Mould, J. R., Hughes, S. M., Ferrarese, L., Phelps, R., Turner, A., Cook, K. H., Ford, H., Hoessel, J. G. & Huchra, J. 1996, ApJ, 463, 26

Lacey, C. K., Weiler, K. W., Van Dyk, S. D., & Sramek, R. A. 1999, BAAS, 31, 976

Leibundgut, B., Kirshner, R. P., Pinto, P. A., Rupen, M. P., Smith, R. C., Gunn, J. E. & Schneider, D. P. 1991, ApJ, 372, 531

Liller, W. 1990, IBVS No. 3497

Long, K. S., Blair, W. P. & Krzeminski, W. 1989, ApJ, 340, L25

Long, K. S., Winkler, P. F., & Blair, W. P. 1992, ApJ, 395, 632

Lundqvist, P. & Fransson, C. 1988, A&A, 192, 221

Madore, B. F. & Freedman, W. L. 1991, PASP, 103, 933

Matonick, D. M. & Fesen, R. A. 1997, ApJS, 112, 49

Montes, M. J., Van Dyk, S. D., Weiler, K. W., Sramek, R. A., & Panagia, N. 1997, ApJ, 482, L61

Montes, M. J., Van Dyk, S. D., Weiler, K. W., Sramek, R. A., Panagia, N., 1998, ApJ, 506, 874

Montes, M. J., Weiler, K. W., Van Dyk, S. D., Panagia, N., Lacey, C. K., Sramek, R. A., & Park, R. 2000, ApJ, 532, ,1124

Mürset, U., Nussbaumer, H., Schmidt, H. M., & Vogel, M. 1991, A&A, 248, 458

Nomoto, K., Iwamoto, K., Suzuki, T., Pols, O. R., Yamaoka, H., Hashimoto, M., Höflich, P., & Van Den Heuvel, E. P. J. 1996, in Compact Stars in Binaries, eds. J. van Paradijs et al., IAU (Netherlands), p. 119

Panagia, N., Sramek, R. A., & Weiler, K. W. 1986, ApJ, 300, L55

Romanishin, W. 1997, private communication

Rupen, M. P., van Gorkom, J. H., Knapp, G. R., Gunn, J. E., & Schneider, D. P. 1987, AJ, 94, 61

Ryder, S., Stavely-Smith, L., Dopita, M., Petre, R., Colbert, E., Malin, D., & Schlegel, E. 1993, ApJ, 416, 167

Saha, A., Labhardt, L., Schwengeler, H., Macchetto, F. D., Panagia, N., Sandage, A., & Tammann, G. A. 1994, ApJ, 425, 14

Saha, A., Sandage, A., Labhardt, L., Schwengler, H. & Machetto, F. D. 1995, ApJ, 438, 8

Saha, A., Sandage, A., Labhardt, L., Tammann, G. A., Macchetto, F. D. & Panagia, N. 1997, ApJ, 486, 1

Sandage, A. & Tammann, G. A., 1974, ApJ, 194, 223

Sandage, A. & Tammann, G. A., 1982, ApJ, 256, 339

Schlegel, E. M. 1990, MNRAS, 244, 269

Schlegel, E. M., Ryder, S., Staveley-Smith, L., Petre, R., Colbert, E., Dopita, M., Campbell-Wilson, D. 1999, AJ, 118, 2689

Seaquist, E. R., & Taylor, A. R. 1990, ApJ, 349, 313

Silbermann, N. A., Harding, P., Madore, B. F., Kennicutt, Jr., R. C., Saha, A., Stetson, P. B., Freedman, W. L., Mould, J. R., Graham, J. A., Hill, R. J., Turner, A., Bresolin, F., Ferrarese, L., Ford, H., Hoessel, J. G., Han, M., Huchra, J., Hughes, S. M. G., Illingworth, G. D., Phelps, R. & Sakai, S. 1996, ApJ, 470, 1

Sivan, J. -P., Petit, H., Compte, G., & Maucherat, A. J. 1990, A&A, 237, 23

Sonneborn, G., Pun, C. S. J., Kimble, R. A., Gull, T. R., Lundqvist, P., McCray, R., Plait, P., Boggess, A., Bowers, C. W., Danks, A. C., Grady, J., Heap, S. R., Kraemer, S., Lindler, D., Loiacono, J., Maran, S. P., Moos, H. W.,& Woodgate, B. E., ApJ, 492, L139

Sramek, R. A., Panagia, N., & Weiler, K. W. 1984, ApJ, 285, L59

Sramek, R. A., Weiler, K. W., Van Dyk, S., & Panagia, N. 1993, in Sub-Arcsecond Radio Astronomy, eds. R. J. Davis & R. S. Booth (Cambridge, Cambridge Un. Press), p. 32

Stockdale, C. J., Goss, W. M., Cowan, J. J., & Sramek, R. A. 2001, ApJ, submitted

Stockdale, C. J., Rupen, M. P., Cowan, J. J., Chu, Y.-H. & Jones, S. 2001, AJ, in press

Tully, R. B. 1988, The Catalog of Nearby Galaxies (Cambridge, Cambridge University Press)

Turner, J. L., & Ho, P. T. 1994, ApJ, 421, 122

Van Dyk, S. D., Weiler, K. W., Sramek, R. A. & Panagia, N. 1992, ApJ, 396, 195

Van Dyk, S. D., Sramek, R. A., Weiler, K. W., & Panagia, N. 1993a, ApJ, 409, 162

Van Dyk, S. D., Weiler, K. W., Sramek, R. A., & Panagia, N., 1993b, ApJ, 419, L69

Van Dyk, S. D., Weiler, K. W., Sramek, R. A., Rupen, M., & Panagia, N., 1994, ApJ, 432, L115

Van Dyk, S. 1997, private communication

Van Dyk, S. D., Montes, M. J., Weiler, K. W., Sramek, R. A., & Panagia, N., 1998, AJ, 115, 1103

Weiler, K. W., Panagia, N., Sramek, R. A., van der Hulst, J. M., Roberts, M. S. & Nguyen, L. 1989, ApJ, 336, 421

Weiler, K. W., Panagia, N. & Sramek, R. A. 1990, ApJ, 364, 611

Weiler, K. W., & Sramek, R. A., 1988, ARAA, 26, 295

Weiler, K. W., Sramek, R. A., Panagia, N., van der Hulst, J. M., & Salvati, M. 1986, ApJ, 301, 790

Weiler, K. W., van Dyk, S. D., Montes, M., Panagia, N., & Sramek, R. A. 1998, ApJ, 500, 51

Weiler, K. W., van Dyk, S. D., Panagia, N., Sramek, R. A., & Discenna, J. L. 1991, ApJ, 380, 161

Weiler, K. W., Van Dyk, S. D., Panagia, N., & Sramek, R. A. 1992a, ApJ, 398, 248

Weiler, K. W., Van Dyk, S. D., Pringle, J. E., & Panagia, N. 1992b, ApJ, 399, 672

Willis, A. G., Oosterbaan, C. E., de Ruiter, H. R. 1976, A&ASup, 25, 453

Zhang, X., Wright, M., Alexander, P. 1993, ApJ, 418, 100

This manuscript was prepared with the AAS LaTeX macros v4.0.

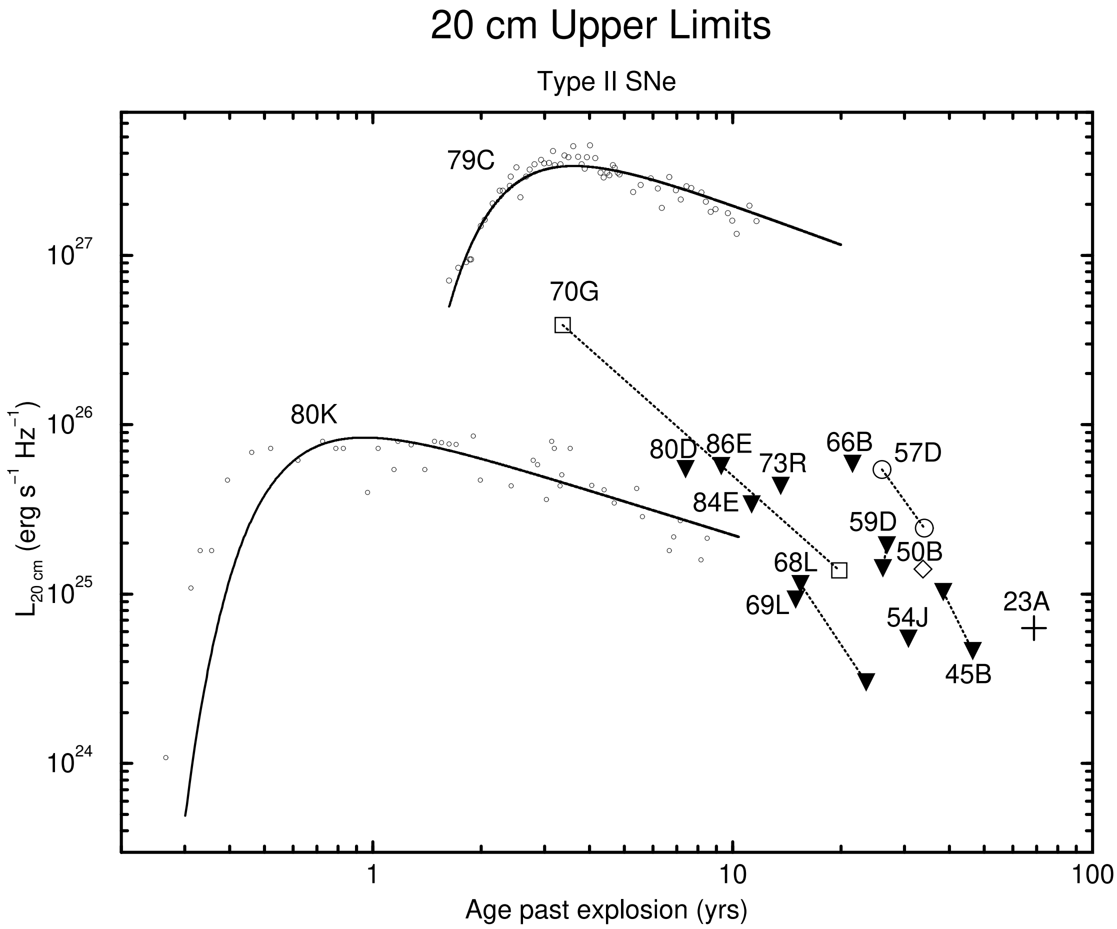

Fig. 1.— A plot of luminosity versus age for the SNe II in our survey at 20 cm. Our upper limits are designated as upside-down triangles, the unfilled shapes (squares for SN 1970G, larger circles for SN 1957D, diamond for SN 1950B, plus sign for SN 1923A) are data for the radio detections in our survey. Included are data (small unfilled circles) and model fits (solid curves) to the data for two well-observed SNe II, SNe 1979C (Weiler et al. [1986,1991]) and 1980K (Weiler et al. [1986,1992a]).

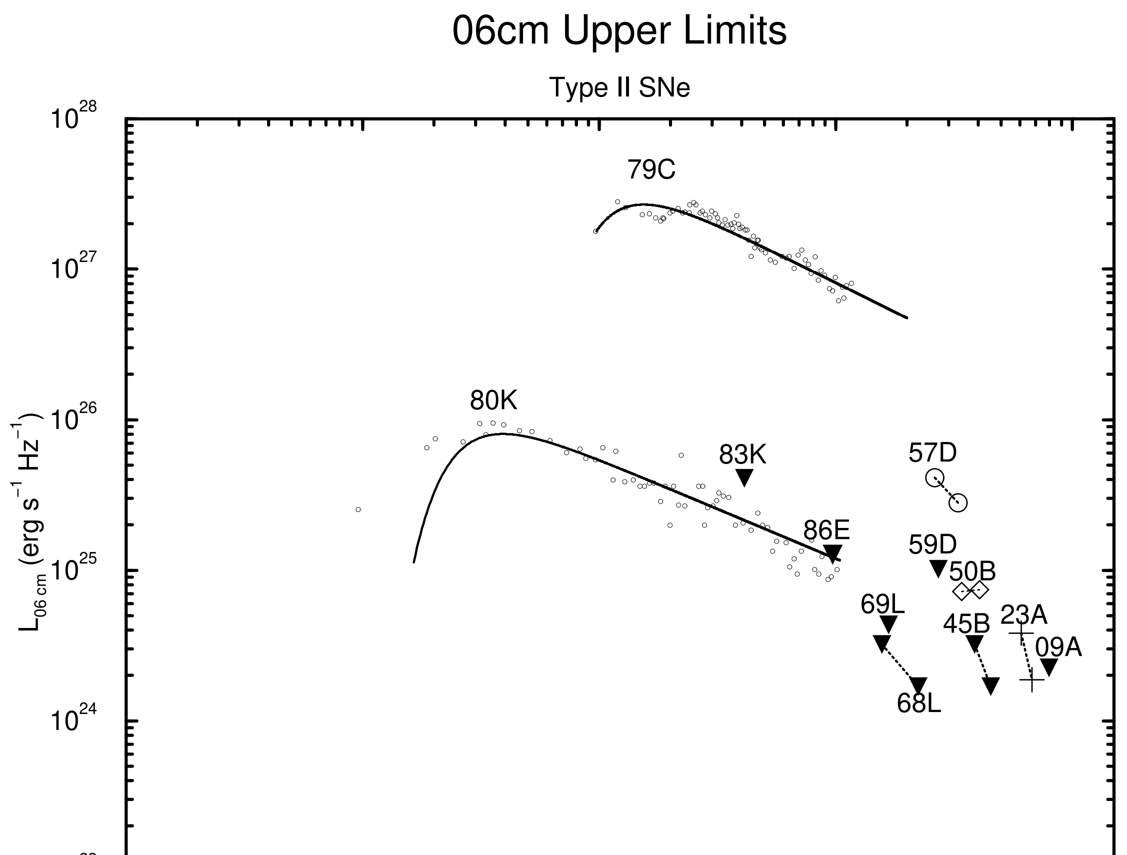

Fig. 2.— A plot of luminosity versus age for the SNe II in our survey at 6 cm. The data and curves are labeled as in Figure 1. The data and light curves for SNe 1979C and 1980K are from Weiler et al. (1986, 1991) and Weiler et al. (1986,1992), respectively.

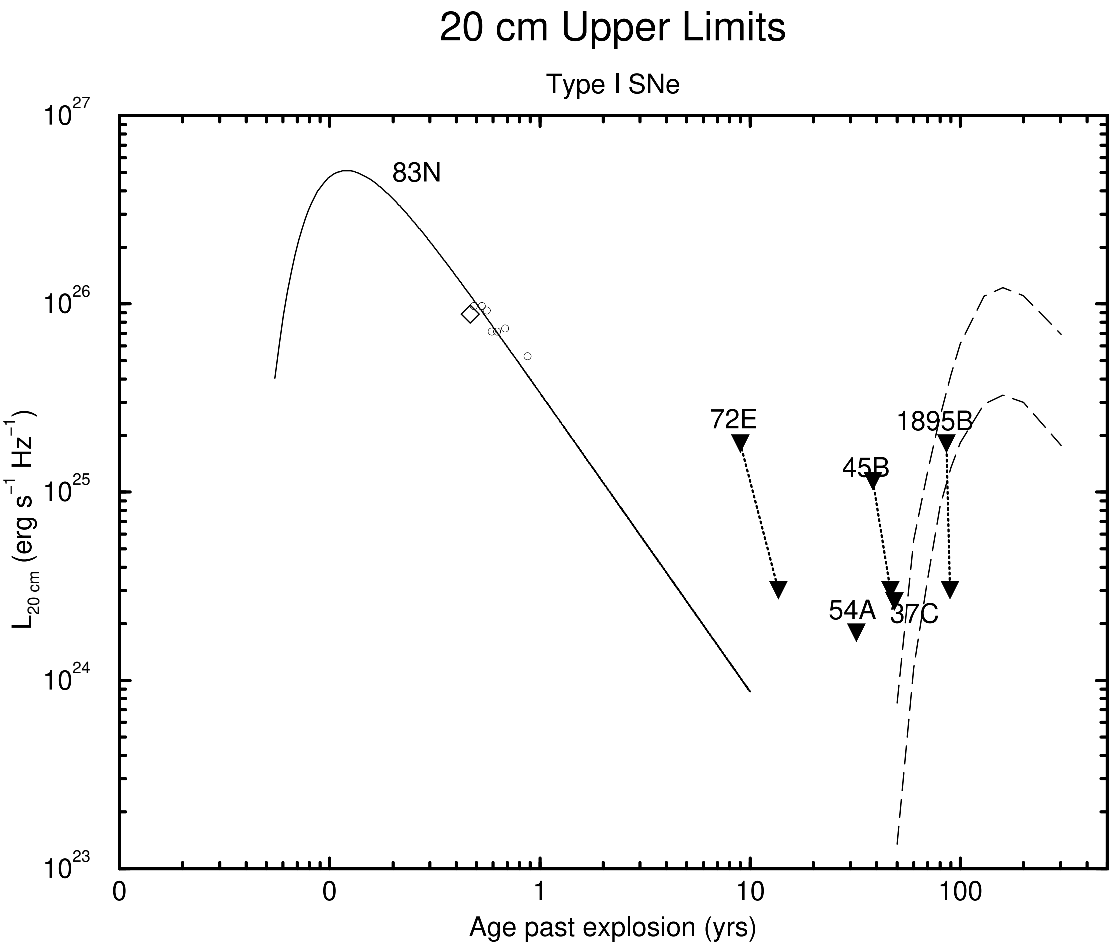

Fig. 3.— A plot of luminosity versus age for the Type I SNe in our survey at 20 cm. Our upper limits are designated as upside-down triangles and the diamond represents our datum for SN 1983N. The smaller unfilled circles and the solid curve are data and a model fit to the data from Weiler et al. (1986) for SN 1983N. The dashed curves are light curves for the onset of the SNR phase from calculations by Cowsik & Sarkar (1984) based on the Gull (1973) model. The two curves are for different model assumptions (see §3.3.2).

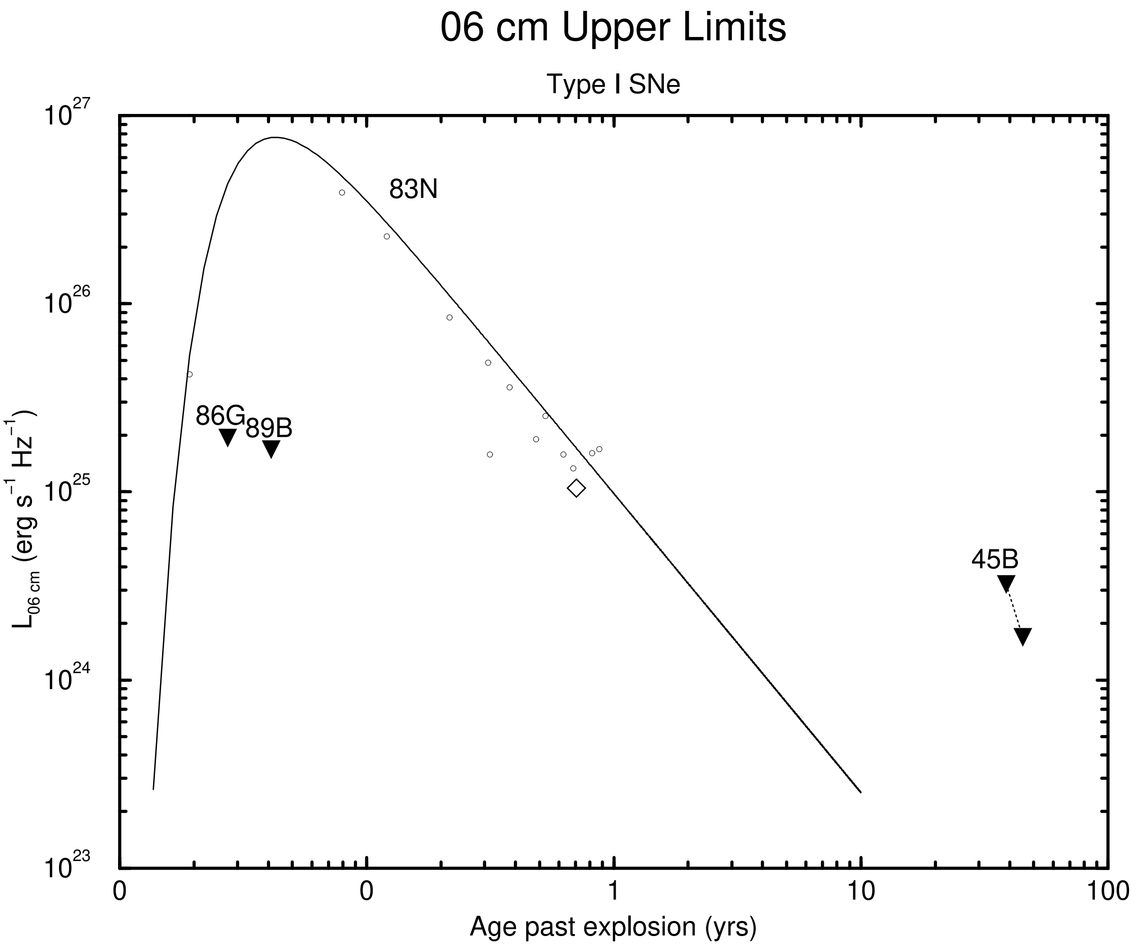

Fig. 4.— A plot of luminosity versus age for the Type I SNe in our survey at 6 cm. Designations are as in Figure 3.

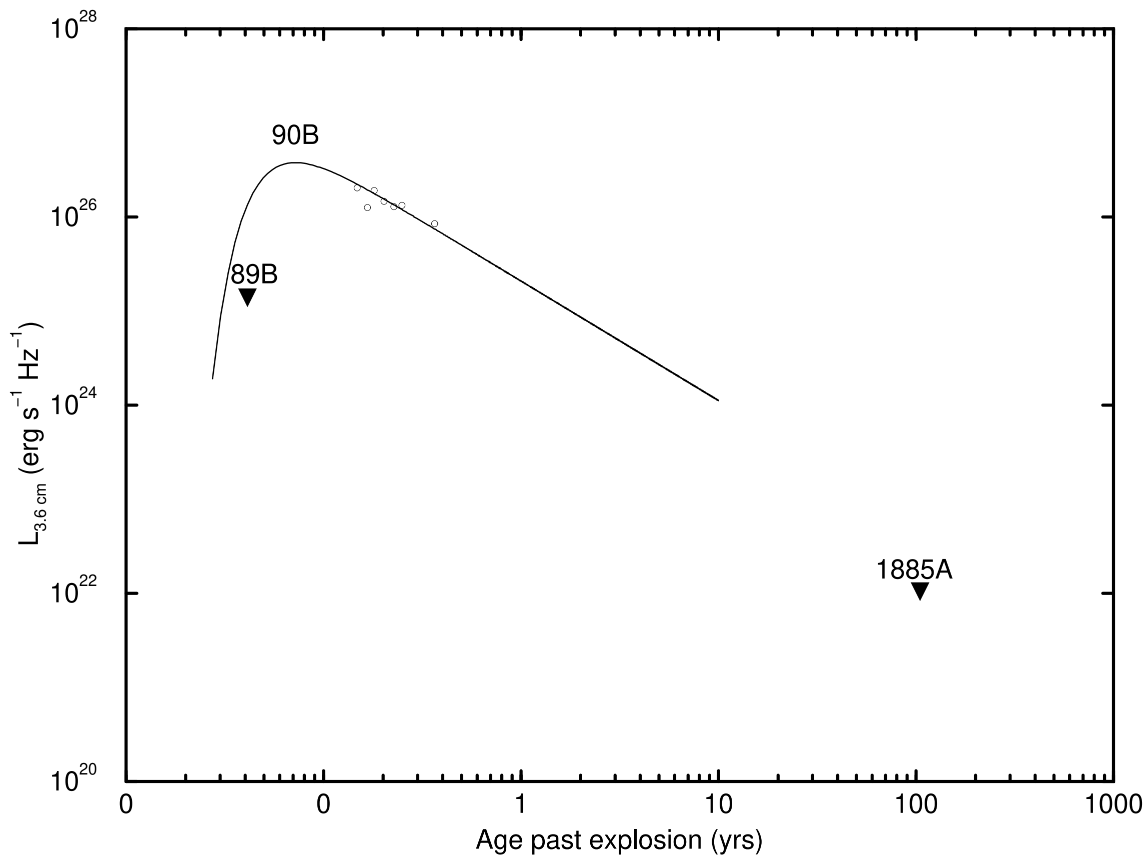

Fig. 5.— A plot of luminosity versus age for the Type I SNe in our survey at 3.6 cm. Upper limits are designated as upside-down triangles. The upper limit for SN 1885A is from Crane et al. (1992). Data (small circles) and light curve (solid curve) are from the Type Ic SN 1990B (Van Dyk et al. 1993a) since data at 3.6 cm was unavailable for SN 1983N.

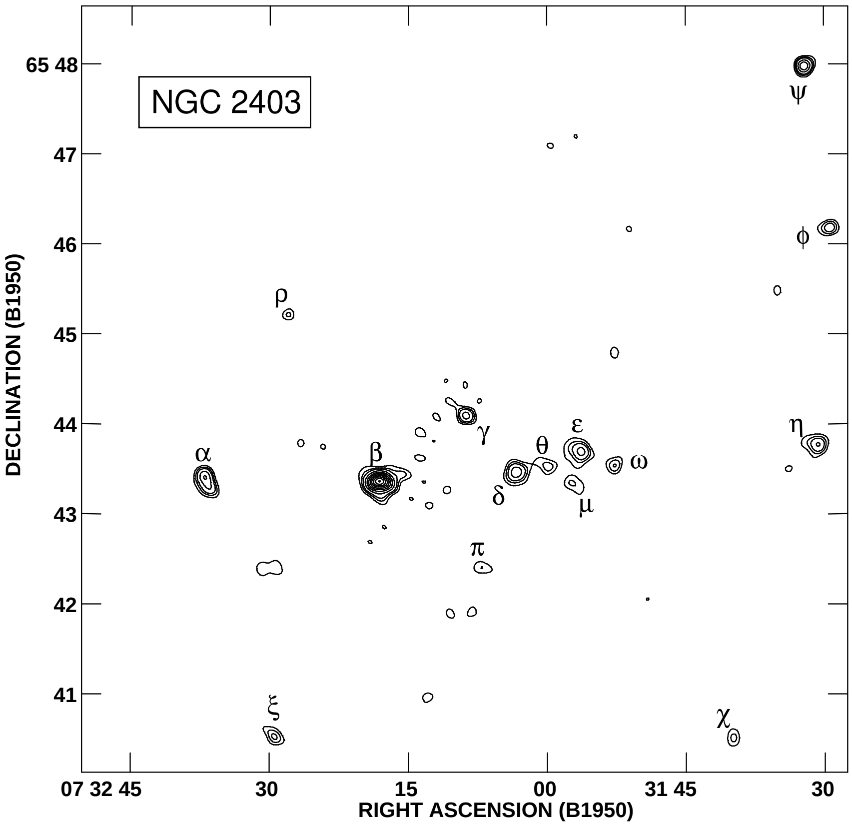

Fig. 6.— A contour map of the field of view for the 15 sources in NGC 2403 at 20 cm, labeled as in Table 5. Sources β, γ, δ, ϵ, ρ, θ, ω, η, χ and ξ are probably H II regions (see text). Contour levels are at 0.47, 0.70, 0.94, 1.4, 1.9, 2.3, 2.8, 3.3, 3.7, 4.2, and 4.6 mJy beam^{-1} and the rms noise is 0.12 mJy beam^{-1}.

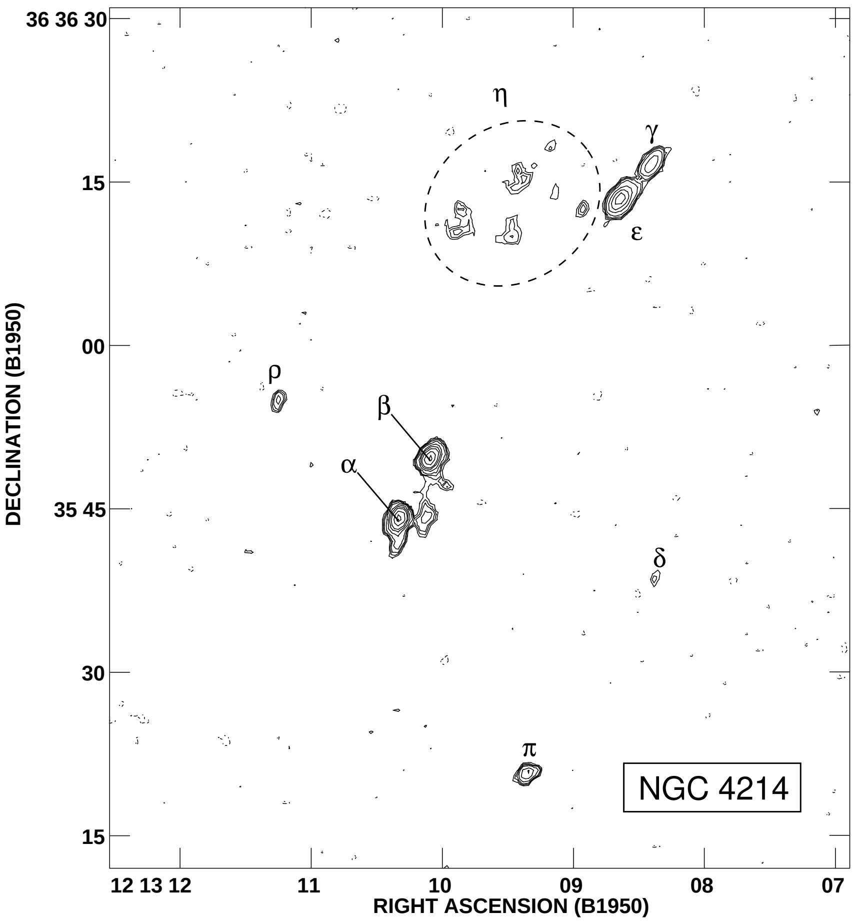

Fig. 7.— A contour map of part of the field of view for NGC 4214 at 20 cm, labeled as in Table 5. The sources that appear to be a part of a larger complex are circled and labeled η. Sources α, β, γ and η are all likely to be H II regions (see text). Contour levels are at -0.053, 0.066, 0.083, 0.099, 0.13, 0.20, 0.27, 0.33, 0.47, 0.60 and 0.66 mJy beam^{-1} and the rms noise is 0.022 mJy beam^{-1}.

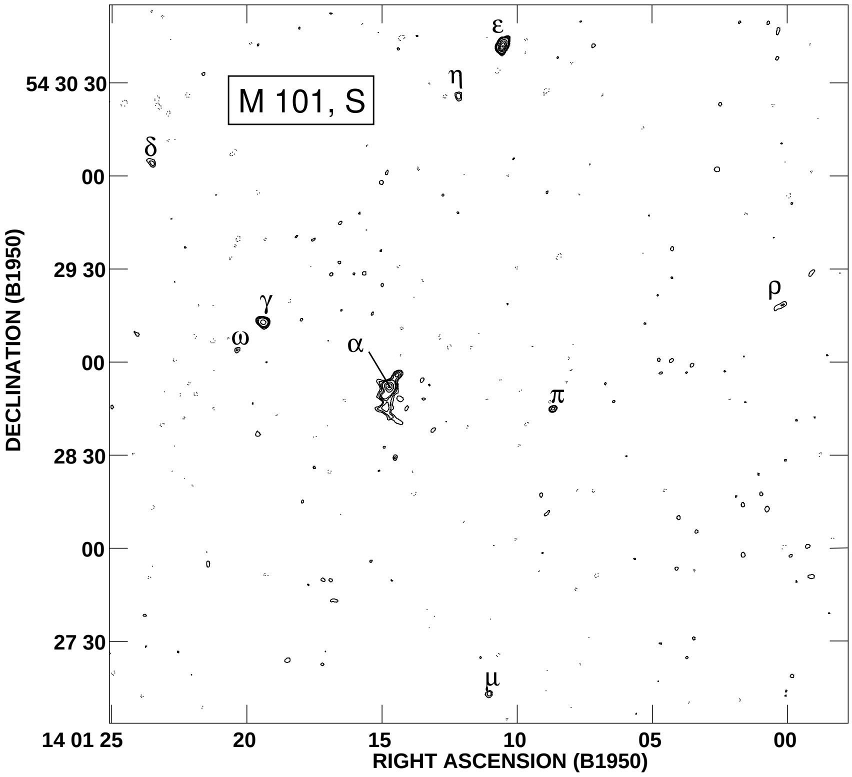

Fig. 8.— A contour map of part of the field of view for the southern region of NGC 5457 (M 101) at 20 cm, labeled as in Table 5. Emission from SN 1970G (source β) is visible just to the northwest of α, but not labeled. Sources α, δ and ω are probably H II regions from their flat spectral indices (see Table 5). Contour levels are at -0.065, 0.065, 0.093, 0.14, 0.19, 0.37, 0.56, 0.74 and 0.92 mJy beam^{-1} and the rms noise is 0.021 mJy beam^{-1}.

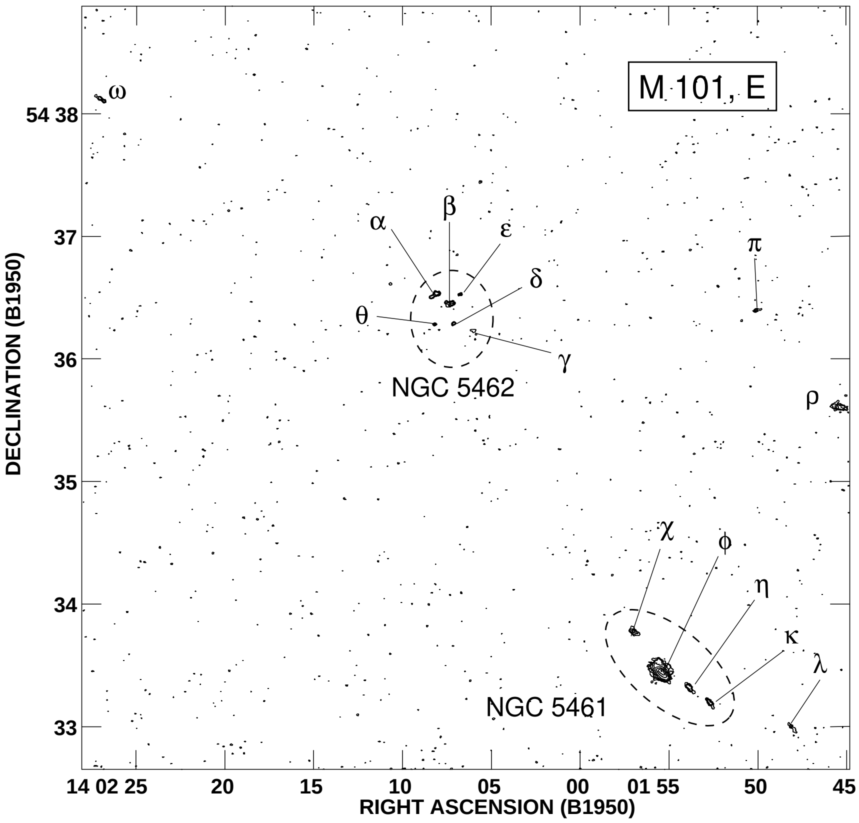

Fig. 9.— A contour map of part of the field of view for the eastern region of NGC 5457 (M 101) at 20 cm, labeled as in Table 5. Clearly visible are the (circled) emission regions associated with NGC 5461 and NGC 5462. The contour levels are at 0.043, 0.064, 0.086, 0.13, 0.21, 0.43, 0.64 and 0.85 mJy beam^{-1} and the rms noise is 0.015 mJy beam^{-1}.